Template banks to search for low-mass binary black holes in advanced gravitational-wave detectors.

Duncan A. Brown, Prayush Kumar, and Alexander H. Nitz
Department of Physics, Syracuse University, Syracuse NY 13244

Coalescing binary black holes (BBHs) are among the most likely sources for the Laser Interferometer Gravitational-wave Observatory (LIGO) and its international partners Virgo and KAGRA. Optimal searches for BBHs require accurate waveforms for the signal model and effectual template banks that cover the mass space of interest. We investigate the ability of the second-order post-Newtonian TaylorF2 hexagonal template placement metric to construct an effectual template bank, if the template waveforms used are effective one body waveforms tuned to numerical relativity (EOBNRv2). We find that by combining the existing TaylorF2 placement metric with EOBNRv2 waveforms, we can construct an effectual search for BBHs with component masses in the range $3M_{\odot} \leq m_1, m_2 \leq 25\,M_{\odot}$. We also show that the (computationally less expensive) TaylorF2 post-Newtonian waveforms can be used in place of EOBNRv2 waveforms when $M \lesssim 12\,M_{\odot}$. Finally, we investigate the effect of modes other than the dominant $l = m = 2$ mode in BBH searches. We find that for systems with $(m_1/m_2) \leq 1.5$, there is no significant loss in the total possible signal-to-noise ratio due to neglecting modes greater than $l = m = 2$ in the template waveforms. For higher mass ratios, including higher order modes could increase the signal-to-noise ratio by as much as 8% in Advanced LIGO. Our results can be used to construct matched-filter in Advanced LIGO and Advanced Virgo.

PACS numbers: 04.80.Nn, 04.25.Nx, 04.30.Db,

I. INTRODUCTION

Over the last decade, there has been tremendous progress towards the first direct detection of gravitational waves. Construction of the Advanced Laser Interferometer Gravitational-Wave Observatory (aLIGO) is underway, with completion scheduled for 2014 [1]. Similar upgrades to the French-Italian Virgo detector [2] have commenced and construction of the Japanese KAGRA detector has begun [3]. When these second-generation gravitational-wave detectors reach design sensitivity, they will increase the observable volume of the universe by a thousandfold or more [4], compared to the first-generation detectors.

The inspiral and merger of binary black holes (BBHs) are expected to be an important source for detection by aLIGO [5]. The rate of BBH coalescences that will be observed by aLIGO at design sensitivity is estimated to be between $0.2\,\mathrm{yr}^{-1}$ and $1000\,\mathrm{yr}^{-1}$ [6]. Accurate knowledge of the gravitational-wave signals generated by BBHs is crucial for detecting and extracting information about these sources. To provide such waveforms, the effective one body (EOB) model [7] has been calibrated to numerical simulations of black hole mergers [8–15]. A new EOB waveform family (called EOBNRv2) has been recently proposed that incorporates information from several non-spinning BBH simulations, with black hole ring-down quasi-normal modes [16, 17] attached to provide a complete BBH waveform [15]. The EOBNRv2 waveform is believed to be sufficiently accurate to search for non-spinning BBH signals in the aLIGO sensitive band (10-1000 Hz).

Past searches for BBHs [18–22] used matched-filtering [23, 24] to search for coalescing compact binaries. These searches divided the BBH mass space into a *low-mass* region with $M = m_1 + m_2 \lesssim 25\,M_{\odot}$ and a *high-mass* region with $M \gtrsim 25\,M_{\odot}$. In this paper, we focus attention on BBH systems with component masses between $3\,M_{\odot} \lesssim m_1, m_2 \lesssim 25M_{\odot}$, which encompasses mass distribution of black hole candidates observed in low-mass X-ray binaries [25]. aLIGO will be able to detect coalescing BBH systems with component masses $m_1 = m_2 = 25\,M_{\odot}$ to a maximum distance of up to ~ 3.6 Gpc. Since we do not know *a priori* the masses of BBHs that gravitational-wave detectors will observe, searches use a *bank* of template waveforms which covers the range of BBH component masses of interest [26, 27]. This technique is sensitive to the accuracy of the waveform templates that are used as filters and the algorithm used to place the template waveforms [28]. An accurate template bank is required as input for matched filter searches in the Fouier domain [24], as well as newer search algorithms such as the singular value decomposition [29].

In this paper, we investigate three items of importance to advanced-detector BBH searches: First, we study the accuracy of template placement algorithms for BBH searches using EOBNRv2 waveforms. Optimal template placement requires a metric for creating a grid of waveforms in the desired region of parameter space [30], however no analytic metric exists for the EOBNRv2 waveform. In the absence of such a metric, we construct a template bank using the second-order post-Newtonian hexagonal placement algorithm [31–34]. This metric is used to place template grid points for the aLIGO zero-detuning high power sensitivity curve [35] and we use EOBNRv2 waveforms at these points as search templates. We find that the existing algorithm works well for BBHs with component masses in the range $3M_{\odot} \leq m_1, m_2 \leq 25\,M_{\odot}$. For a template bank constructed with a minimal match of 97% less than 1.5% of non-spinning BBH signals have a mismatch greater than 3%. We therefore conclude that the existing bank placement algorithm is sufficiently accurate for non-spinning BBH searches in this mass region. Second, we investigate the mass range in which the (computationally less expensive) third-and-a-half-order TaylorF2 post-Newtonian waveforms [26, 36–44] can be used without significant loss in event rate, and where full inspiral-merger-ringdown EOBNRv2 waveforms are required. We

construct a TaylorF2 template bank designed to lose no more than 3% of the matched filter signal-to-noise ratio and use the EOBNRv2 model as signal waveforms. We find that for non-spinning BBHs with $M \lesssim 12\,M_\odot$, the TaylorF2 search performs as expected, with a loss of no more than 10% in the event rate. For higher masses larger event rate losses are observed. A similar study was performed in Ref. [45] using an older version of the EOB model and our results are quantitatively similar. We therefore recommend that this limit is used as the boundary between TaylorF2 and EOBNRv2 waveforms in Advanced LIGO searches. Finally, we investigate the effect of modes other than the dominant $l = m = 2$ mode on BBH searches in aLIGO. The horizion distance of aLIGO (and hence the event rate) is computed considering only the dominant mode of the emitted gravitational waves, since current searches only filter for this mode [6]. However, the inclusion of sub-dominant modes in gravitational-wave template could increase the reach of aLIGO [46, 47]. If we assume that BBH signals are accurately modeled by the EOBNRv2 waveform including the five leading modes, we find that for systems with $(m_1/m_2) \leq 1.5$, there is no significant loss in the total possible signal-to-noise ratio due to neglecting modes other than $l = m = 2$ in the template waveforms, if one uses a 97% minimal-match bank placed using the TaylorF2 metric. However, for higher mass ratios, including higher order modes could increase the signal-to-noise ratio by as much as 8% in aLIGO. This increase in amplitude may be offset by the increase in false alarm rate from implementing searches which also include sub-dominant waveform modes in templates, so we encourage the investigation of such algorithms in real detector data.

The remainder of this paper is organized as follows: In Sec. II we review the gravitational waveform models used in this study. In Sec. III we present the results of large-scale Monte Carlo signal injections to test the effectualness of the template banks under investigation. Finally in Sec. IV we review our findings and reccomendations for future work.

II. WAVEFORMS

The dynamics of a BBH system can be broadly divided into three regimes: (i) The early inspiral, when the separation between the black holes is large and their velocity is small, can be modeled using results from post-Newtonian (PN) theory [48]. The gravitational-wave phasing of non-spinning binaries is available up to 3.5PN order [38–44]. (ii) Accurately modeling the late-inspiral and merger requires the numerical solution of the Einstein equations [49–55]. (iii) The final ring-down phase can modeled using a super-position of quasi-normal modes (QNMs) which describe the oscillations of the perturbed Kerr black-hole that is formed from the coalescence [16, 17].

Numerical simulation of BBH systems are computationally expensive, and results are only available for a relatively small number of binary systems (see e.g. [56]). The EOB model [7] provides a framework for computing the gravitational waveforms emitted during the inspiral and merger of BBH systems. By attaching a QNM waveform and calibrating the model to numerical relativity (NR) simulations, the EOB framework provides for accurate modeling of complete BBH waveforms (EOBNR). The EOBNR waveforms can be computed at relatively low cost for arbitrary points in the waveform parameter space [8–15]. In particular the EOB model has recently been tuned against high-accuracy numerical relativity simulations of non-spinning BBHs of mass-ratios $q = \{1, 2, 3, 4, 6\}$, where $q \equiv m_1/m_2$ [15]; we refer to this as the EOBNRv2 model, which we review the major features of below. Throughout, we set $G = c = 1$.

The EOB approach maps the fully general-relativistic dynamics of the two-body system to that of an *effective* mass moving in a deformed Schwarzschild spacetime [7]. The physical dynamics is contained in the deformed-spacetime's metric coefficients, the EOB Hamiltonian [7], and the radiation-reaction force. In polar coordinates (r, Φ), the EOB metric is written as

$$\mathrm{d}s^2_{\text{eff}} = -A(r)\mathrm{d}t^2 + \frac{A(r)}{D(r)}\mathrm{d}r^2 + r^2\left(\mathrm{d}\Theta^2 + \sin^2\Theta\mathrm{d}\Phi^2\right). \tag{1}$$

The geodesic dynamics of the *effective* mass $\mu = m_1 m_2/M$ in the background of Eq. (1) is described by an effective Hamiltonian H^{eff} [7, 57]. The EOBNRv2 model uses Pade-resummations of the third-order post-Newtonian Taylor expansions of the metric coefficients $A(r)$ and $D(r)$, with additional 4PN and 5PN coefficients that are calibrated [9–12, 15] to ensure that the dynamics agrees closely with NR simulations of comparable mass binaries.

Gravitational waves carry energy and angular momentum away from the binary, and the resulting radiation-reaction force $\hat{F}_\Phi$ causes the orbits to shrink. This is related to the energy flux as

$$\hat{F}_\Phi = -\frac{1}{\eta\hat{\Omega}}\frac{\mathrm{d}E}{\mathrm{d}t} = -\frac{1}{\eta v^3}\frac{\mathrm{d}E}{\mathrm{d}t}, \tag{2}$$

where, $v = (\hat{\Omega})^{1/3} = (\pi M f)^{1/3}$ and f is the instantaneous gravitational-wave frequency. The energy flux $\mathrm{d}E/\mathrm{d}t$ is obtained by summing over the contribution from each term in the multipole expansion of the waveform, i.e.

$$\frac{\mathrm{d}E}{\mathrm{d}t} = \frac{\hat{\Omega}^2}{8\pi}\sum_l\sum_m\left|\frac{\mathcal{R}}{M}h_{lm}\right|^2. \tag{3}$$

$\mathcal{R}$ is the physical distance to the binary, and h_{lm} are the multipoles of the waveform when it is decomposed in spin weighted spherical harmonic basis according to

$$h_+ - \mathrm{i}h_\times = \frac{M}{\mathcal{R}}\sum_{l=2}^{\infty}\sum_{m=-l}^{m=l} Y^{lm}_{-2}\, h_{lm}, \tag{4}$$

where Y^{lm}_{-2} are the spin weighted spherical harmonics, and h_+ and $h_\times$ are the two orthogonal gravitational wave polarizations. These waveform multipoles depend on the coordinates and their conjugate momenta, and their Taylor expansions were re-summed as products of individually re-summed

factors [58],

$$h_{lm} = h^F_{lm} N_{lm}, \tag{5a}$$

$$h^F_{lm} = h^{(N,\epsilon)}_{lm} \hat{S}^{(\epsilon)}_{\rm eff} T_{lm} e^{\mathrm{i}\delta_{lm}} (\rho_{lm})^l; \tag{5b}$$

where ϵ is 0 if $(l+m)$ is even, and is 1 otherwise. This factorized-re-summation of the waveform multipoles ensures agreement with NR waveform multipoles [8–10]. The first factor $h^{(N,\epsilon)}_{lm}$ is the re-summation of the Newtonian order contribution and the second factor $\hat{S}^{(\epsilon)}_{\rm eff}$ is the source term, given by the mass or the current moments of the binary in the EOB formalism [58, 59]. The tail term T_{lm} is the re-summation of the leading order logarithmic terms that enter into the transfer function of the near-zone multipolar waves to the far-zone [59]. The last term N_{lm} attempts to capture the non-circularity of the quasi-circular orbits. While calculating the energy flux in this study we follow exactly the prescription of Ref. [15], which calibrates the coefficients of the flux so that resulting EOB waveform multipoles reproduce their NR counterparts with high accuracy.

We use the EOBNRv2 Hamiltonian and flux in the equations of motion for the binary, given by

$$\frac{\mathrm{d}r}{\mathrm{d}\hat{t}} \equiv \frac{\partial \hat{H}^{\rm real}}{\partial p_r} = \frac{A(r)}{\sqrt{D(r)}} \frac{\partial \hat{H}^{\rm real}}{\partial p_{r*}}(r, p_{r*}, p_\Phi), \tag{6}$$

$$\frac{\mathrm{d}\Phi}{\mathrm{d}\hat{t}} \equiv \hat{\Omega} = \frac{\partial \hat{H}^{\rm real}}{\partial p_\Phi}(r, p_{r*}, p_\Phi), \tag{7}$$

$$\frac{\mathrm{d}p_{r_*}}{\mathrm{d}\hat{t}} = -\frac{A(r)}{\sqrt{D(r)}} \frac{\partial \hat{H}^{\rm real}}{\partial r}(r, p_{r*}, p_\Phi), \tag{8}$$

$$\frac{\mathrm{d}p_\Phi}{\mathrm{d}\hat{t}} = \hat{F}_\Phi(r, p_{r*}, p_\Phi); \tag{9}$$

where, $\hat{t}\,(\equiv\ t/M)$ is time in dimensionless units. Starting from the initial coordinate configuration calculated for a fiduciary starting gravitational wave frequency, we numerically integrate these equations to get the evolution of the coordinates and momenta $(r(t), \Phi(t), p_r(t), p_\Phi(t))$ over the course of inspiral, until the light-ring is reached. In the EOB model, the light-ring is defined as the local maximum of the orbital frequency $\hat{\Omega}$. From the coordinate evolution, we also calculate $h^F_{lm}(t)$, which is the analytic expression for the waveform multipole without the non-quasi-circular correction factor (defined in Eq. (5b)). While generating $h^F_{lm}(t)$ from the dynamics, the values for the free parameters in the expressions for δ_{lm} and ρ_{lm}, are taken from Eqn.[38a-19b] of Ref. [15], where they optimize these parameters to minimize the phase and amplitude discrepancy between the respective EOB waveform multipoles and those extracted from NR simulations.

The EOB ringdown waveform is modeled as a sum of N quasi-normal-modes (QNMs) [9, 10, 12, 16]

$$h^{\rm RD}_{lm}(t) = \sum_{n=0}^{N-1} A_{lmn} e^{-\mathrm{i}\sigma_{lmn}(t - t^{\rm match}_{lm})}, \tag{10}$$

where $N = 8$ for the model we consider. The matching time $t^{\rm match}_{lm}$ is the time at which the inspiral-plunge and the ringdown waveforms are attached and is chosen to be the time at which the amplitude of the inspiral-plunge part of $h_{lm}(t)$ peaks $\left(\text{i.e.}\, t^{lm}_{\rm peak}\right)$ [9, 15]. The complex frequencies of the modes σ_{lmn} depend on the mass M_f and spin a_f of the BH that is formed from the coalescence of the binary. We use the relations of Ref. [15], given by

$$\frac{M_f}{M} = 1 + \left(\sqrt{\frac{8}{9}} - 1\right)\eta - 0.4333\eta^2 - 0.4392\eta^3, \tag{11a}$$

$$\frac{a_f}{M} = \sqrt{12}\eta - 3.871\eta^2 + 4.028\eta^3. \tag{11b}$$

Using the mass and spin of the final BH, the complex frequencies of the QNMs can be obtained from Ref. [16], where these were calculated using perturbation theory. The complex amplitudes A_{lmn} are determined by a hybrid-comb numerical matching procedure described in detail in Sec.II C of Ref. [15].

Finally, we combine the inspiral waveform multipole $h_{lm}(t)$ and the ringdown waveform $h^{\rm RD}(t)$ to obtain the complete inspiral-merger-ringdown EOB waveform $h^{\rm IMR}(t)$,

$$h^{\rm IMR}_{lm}(t) = h_{lm}(t)\Theta(t^{\rm match}_{lm} - t) + h^{\rm RD}(t)\Theta(t - t^{\rm match}_{lm}), \tag{12}$$

where $\Theta(x) = 1$ for $x \geq 0$, and 0 otherwise. These multipoles are combined to give the two orthogonal polarizations of the gravitational waveform, h_+ and $h_\times$,

$$h_+ - \mathrm{i}h_\times = \frac{M}{\mathcal{R}} \sum_l \sum_m Y^{lm}_{-2}(\iota, \theta_c) h^{\rm IMR}_{lm}, \tag{13}$$

where ι is the inclination angle that the binary's angular momentum makes with the line of sight, and θ_c is a fiduciary phase angle. To ensure the correctness of our results, we wrote independent code to implement the EOBNRv2 waveform based solely on the content of Ref. [15]. We then validated our code against the EOBNRv2 waveform algorithm in the LSC Algorithm Library (LAL) [60]. We find agreement between these two implementations, giving us confidence in both our results and the correctness of the LAL EOBNRv2 code.

Previous searches for stellar-mass BBHs with total mass $M \lesssim 25 M_\odot$ in LIGO and Virgo used the restricted TaylorF2 PN waveforms [26, 36, 37]. Since this waveform is analytically generated in the frequency domain, it has two computational advantages over the EOBNRv2 model: First, the TaylorF2 model does not require either the numerical solution of coupled ODEs or a Fourier transform to generate the frequency domain signal requred by a matched filter. We compared the speed of generating and Fourier transforming EOBNRv2 waveforms, to the speed of generating Taylor F2 waveforms in the frequency domain, and found that the former can be $\mathcal{O}(10^2)$ times slower than the latter. Second, the TaylorF2 model can be implmented trivially as a kernel on Graphics Processing Units, allowing search pipelines to leverage significant speed increases due to the fast floating-point performance of GPU hardware. We found the generation of TaylorF2 waveforms using GPUs to be $\mathcal{O}(10^4)$ times faster than generating and Fourier transforming EOBNRv2 waveforms on CPUs. However, use of the TaylorF2 waveform

may result in a loss in search efficiency due to inaccuracies of the PN approximation for BBHs. To investigate the loss in search efficiency versus computational efficiency, we use the restricted TaylorF2 waveform described below.

The Fourier transform of a gravitational waveform $h(t)$ is defined by

$$\tilde{h}(f) = \int_{-\infty}^{\infty} e^{-2\pi \mathrm{i} f t} h(t) \mathrm{d}t. \tag{14}$$

Using the stationary phase approximation [61], the Taylor F2 waveform $\tilde{h}(f)$ can be written directly in the frequency domain as

$$\tilde{h}(f) = A f^{-7/6} e^{\mathrm{i}\Psi(f)}, \tag{15}$$

where we have kept only the leading-order amplitude terms; this is known as the restricted PN waveform. The amplitude $A \propto \mathcal{M}_c^{5/6}/\mathcal{R}$, where $\mathcal{M}_c$ is the *chirp-mass* of the binary, $\mathcal{M}_c = (m_1 + m_2)\,\eta^{3/5}$, $\eta = m_1 m_2/(m_1 + m_2)^2$ is the symmetric mass ratio, and $\mathcal{R}$ is the distance to the binary. The Fourier phase of the waveform at 3.5PN order is given by [24, 26, 36, 62–65]

$$\begin{aligned}\Psi(f) =& 2\pi f t_c - \phi_c - \frac{\pi}{4} + \frac{3}{128}\frac{1}{\eta} v^{-5} \left[1 + \left(\frac{3715}{756} + \frac{55}{9}\eta \right) v^2 \right. \\ & - 16\pi v^3 + \left(\frac{15293365}{508032} + \frac{27145}{504}\eta + \frac{3085}{72}\eta^2 \right) v^4 \\ & + \left(\frac{38645}{756} - \frac{65}{9}\eta \right) \left(1 + 3\log\left(\frac{v}{v_{\rm lso}} \right) \right) \pi v^5 \\ & + \left[\frac{11583231236531}{4694215680} - \frac{640}{3}\pi^2 - \frac{6848}{21}\gamma_E \right. \\ & - \frac{6828}{21}\log(4v) + \left(-\frac{15737765635}{3048192} + \frac{2255}{12}\pi^2 \right) \eta \\ & \left. + \frac{76055}{1728}\eta^2 - \frac{127825}{1296}\eta^3 \right] v^6 \\ & \left. + \left(\frac{77096675}{254016} + \frac{378515}{1512}\eta - \frac{74045}{756}\eta^2 \right) \pi v^7 \right],\end{aligned} \tag{16}$$

where $v = (\pi M f)^{1/3}$ is the characteristic velocity of the binary, and γ is Euler's constant. The initial conditions are set by starting the waveform from a given gravitational-wave frequency $f = f_{\rm low}$ and the waveform is terminated at the frequency of a test particle at the innermost stable circular orbit (ISCO) of a Schwarzschild black hole ($r = 6M$).

III. RESULTS

To assess the effectualness of the template banks constructed here, we compute the fitting factors [28] of the template bank, defined as follows. The frequency weighted overlap between two waveforms h_1 and h_2 is given by

$$(h_1|h_2) \equiv 2 \int_{f_{\rm min}}^{\infty} \frac{\tilde{h}_1^*(f)\tilde{h}_2(f) + \tilde{h}_1(f)\tilde{h}_2^*(f)}{S_n(f)} \mathrm{d}f, \tag{17}$$

where $S_n(f)$ is the one-sided power spectral density (PSD) of the detector noise. Throughout, we use the aLIGO zero-detuning high power noise curve as the PSD for bank placement and overlap calculations, and set $f_{\rm min} = 15$ Hz. The normalized overlap between the two waveforms is given by

$$(\hat{h}_1|\hat{h}_2) = \frac{(h_1|h_2)}{\sqrt{(h_1|h_1)(h_2|h_2)}}. \tag{18}$$

In addition to the two mass-parameters of the binary, this normalized overlap is also sensitive to the relative phase of coalescence ϕ_c and to the difference in the time of coalescence between the two waveforms h_1 and h_2, t_c. These two parameters (ϕ_c and t_c) can be analytically maximized over to get the maximized overlap $\mathcal{O}$

$$\mathcal{O}(h_1, h_2) = \max_{\phi_c, t_c} \left(\hat{h}_1 | \hat{h}_2(\phi_c, t_c) \right), \tag{19}$$

which gives a measure of how "close" the two waveforms are in the waveform manifold. The mismatch M between the same two waveforms is written as,

$$M(h_1, h_2) = 1 - \mathcal{O}(h_1, h_2). \tag{20}$$

If h_a^e is the waveform emitted by a BBH system then the *Fitting Factor* of a bank of template waveforms (modeled using approximant X) for this waveform, is defined as the maximum value of maximized normalized overlaps between h_a^e and all members $h_b^{\rm X}$ of the bank of template waveforms [28]; i.e.

$$\mathcal{FF}(a, {\rm X}) = \max_{b \,\in\, \rm bank} \mathcal{O}(h_a^e, h_b^{\rm X}). \tag{21}$$

This quantity simultaneously quantifies the loss in recovered signal-to-noise ratio (SNR) due to the discreteness of the bank, and the inaccuracy of the template model. The similarly defined quantity MM (minimal match) quantifies the loss in SNR due to only the discreteness of the bank as both the *exact* and the template waveform is modeled with the same waveform model, i.e.

$$\mathrm{MM} = \min_a \max_{b \,\in\, \rm bank} \mathcal{O}(h_a^{\rm X}, h_b^{\rm X}), \tag{22}$$

where a is any point in the space covered by the bank, and X is the waveform approximant. For a detection search that aims at less than 10% (15%) loss in event detection rate due to the discreteness of the bank and the inaccuracy of the waveform model, we require a bank of template waveforms that has $\mathcal{FF}$ above 0.965 (0.947) [45, 66, 67].

A. EOBNRv2 templates placed using TaylorF2 metric

In this section we measure the effectualness of the second-order post-Newtonian hexagonal template bank placement metric described in Ref. [32] when used to place EOBNRv2 waveform templates for aLIGO. The same template placement algorithm was used to place a grid of third-and-a-half order post-Newtonian order TaylorF2 waveforms for low-mass

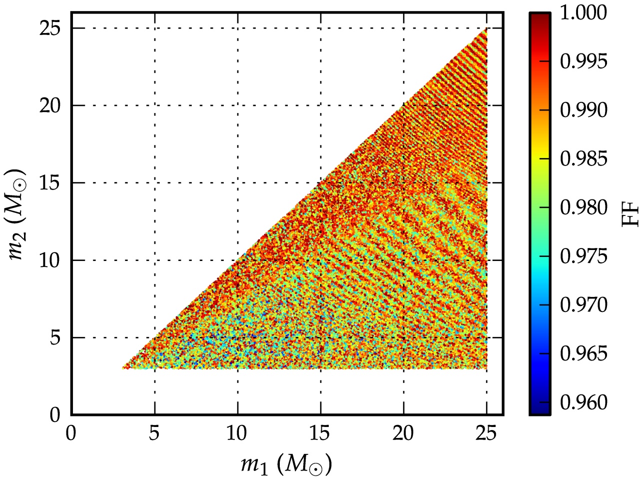

FIG. 1. This figure shows the effectualness of a bank of EOBNRv2 templates, placed using the 2PN accurate hexagonal template placement of Ref. [32], to search for a population of BBH signals simulated with EOBNRv2 waveforms. The masses of the BBH population are chosen from a uniform distribution of component masses between 3 and 25 $M_\odot$. For each injection, we plot the component masses of the injection, and the fitting factor ($\mathcal{FF}$).

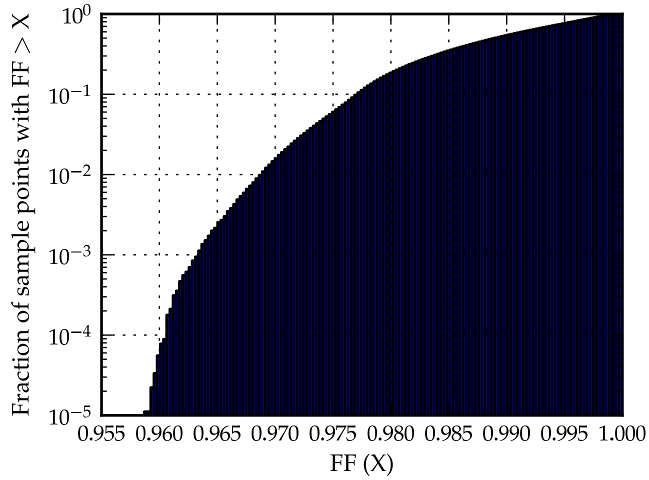

FIG. 2. This figure shows a cumulative histogram of the fraction of the BBH signal space (on the y-axis), where the bank of EOBNRv2 waveforms has $\mathcal{FF}$ less than the respective values on the x-axis. The EOBNRv2 bank has a fitting factor $\mathcal{FF}$ below the 0.97 for less than $\sim$ 1.5% of all simulated signals with component-masses m_1, m_2 between 3 $M_\odot$ and 25 $M_\odot$.

BBH detection searches for initial LIGO and Virgo observations [18–22]. We construct a template bank which has a desired minimal match of 0.97 for waveforms with component masses between $3M_\odot \leq m_1, m_2 \leq 25M_\odot$. This template bank contains 10,180 template grid points in (m_1, m_2) space for the aLIGO noise curve, compared to 373 grid points for the initial LIGO design noise curve. For the template waveforms at each grid point, we use the EOBNRv2 waveforms, rather than TaylorF2 waveforms. Since the metric itself was derived using second-order TaylorF2 waveforms, we do not, *a priori* know if this metric is a good measure to use to place template banks for EOBNRv2 waveforms.

To test the effectualness of this template bank, we perform a Monte-Carlo simulation over the $3M_\odot \leq m_1, m_2 \leq 25M_\odot$ BBH mass space to find regions where the bank placement algorithm leads to under-coverage. We sample 90,000 points uniformly distributed in individual component masses. For each of these points, we generate an EOBNRv2 waveform for the system with component masses given by the coordinates of the point. We record the $\mathcal{FF}$ of the template bank for each of the randomly generated BBH waveforms in the Monte-Carlo simulation. Since we use EOBNRv2 waveforms both to model the true BBH signals and as matched-filter templates, any departure in fitting factor from unity is due to the placement of the template bank grid.

For a bank of template waveforms constructed with a MM of 0.97, Fig. 1 and Fig. 2 show that the $\mathcal{FF}$ of the bank remains above 0.97 for $\sim$ 98.5% of all simulated BBH signals. Less than $\sim$ 1.5% of signals have a minimal match of less than 0.97, with the smallest value over the 90,000 sampled points being $\sim$ 0.96. The diagonal features observed in Fig. 1 are due to the hexagonal bank placement algorithm and are related to the ellipses of constant chirp mass in Fig. 4 of Ref. [32]. From these results, we conclude that the existing template bank placement metric adequately covers the BBH mass space with EOBNRv2 waveform templates; it is not necessary to construct a metric specific to the EOBNRv2 model. aLIGO detection searches can employ the second-order post-Newtonian bank placement metric with the hexagonal placement algorithms [30–34] to place template banks for EOBNRv2 waveforms without a significant drop in the recovered signal-to-noise ratio.

B. Effectualness of TaylorF2 templates

We next explore the efficiency of using the computationally cheaper TaylorF2 waveforms to search for a population of BBH signals with component masses between $(3–25)M_\odot$. The signals from this population are modeled with the full EOBNRv2 waveforms. We use the same template bank placement as above, however now we use the third-and-a-half PN order TaylorF2 model as the template waveforms. This model does not capture the merger and ringdown of BBH signals, as it is terminated at the Schwarzchild test-particle ISCO. Furthermore, it diverges from the true BBH signal in the late inspiral. It is important to determine when these effects become important.

We sample the $(3–25)M_\odot$ BBH component mass space at 25,000 points by generating an EOBNRv2 waveform to generate the "true" signal waveform. We generate a bank of Tay-

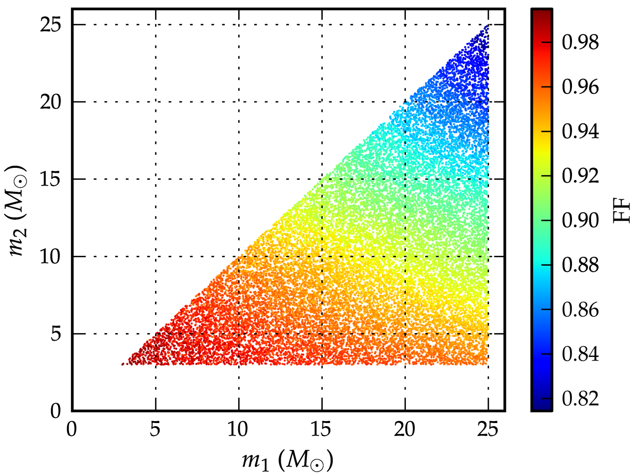

FIG. 3. The fitting factor $\mathcal{FF}$ of a bank of Taylor F2 waveforms, constructed with $\mathrm{MM} = 0.97$ used to search for BBH systems modeled using EOBNRv2 signals. Each point corresponds to a simulated signal and the color bar shows the measured $\mathcal{FF}$ for that signal.

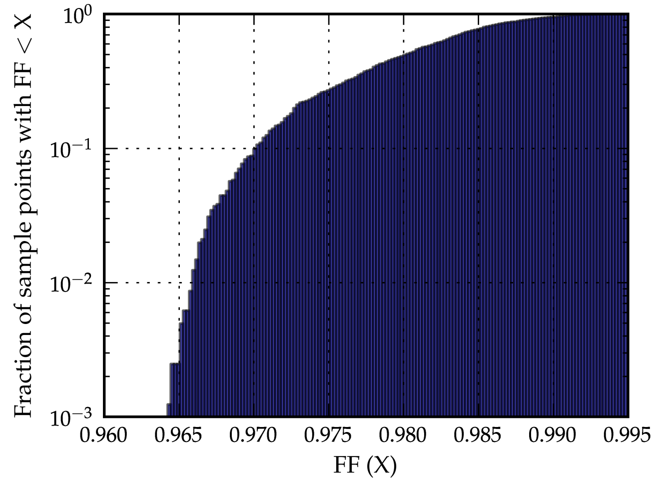

FIG. 4. This figure shows the cumulative histogram of the the fitting factors of a bank of TaylorF2 waveforms against EOBNRv2 waveforms. The points shown here cover only the component mass region with total masses below $12 M_\odot$.

lorF2 template waveforms over the same region, and calculate its $\mathcal{FF}$ for each of the sample points, against the corresponding EOBNRv2 waveform. Fig. 3 shows the distribution of the $\mathcal{FF}$ obtained for the TaylorF2 bank. Clearly the TaylorF2 bank is not effectual for the enture BBH region considered, with mismatches of up to 18% observed. In Fig. 4 we restrict the region of the BBH space to signals with total mass $M \leq 12 M_\odot$. We find that the TaylorF2 template bank has $\mathcal{FF}$ above ~ 0.965 for $\geq 99.5\%$ of the points sampled in this restricted region. We conclude that the TaylorF2 bank is effectual for BBH signals below $12 M_\odot$.

The value of our limit on total-mass is in agreement with the previous study in Ref. [45], however this analysis used the EOBNRv1 model [68] and an older version of the Advanced LIGO noise curve [45]. This agreement provides confidence that this limit will be robust in aLIGO searches and we propose this limit as the upper cutoff for the computationally cheaper TaylorF2 search. To investigate the loss in the $\mathcal{FF}$ due to the mismatch in the template and signal waveform models, we also performed a Monte-Carlo simulation using a denser TaylorF2 bank with $\mathrm{MM} = 0.99$. We found that using this dense bank of third-and-a-half order TaylorF2 waveforms, we can relax the limit on the upper mass to $16 M_\odot$ and still achieve a $\mathcal{FF}$ above 0.965, for over 99.8% of the signals sampled in the region. However, increasing the minimal match increases the size of the template bank from $10,180$ to $27,882$ templates. This is a significant increase, compared to the cost of filtering with EOBNRv2 templates.

C. Effect of sub-dominant modes

Having established that the second-order post-Newtonian hexagonal template bank is effectual for placing a bank of EOBNRv2 templates, we now investigate the effect of neglecting sub-dominant modes in BBH searches. The sensitivity reach of the aLIGO detectors is normally computed assuming that the search is only sensitive to the dominant $l = m = 2$ mode of the gravitational waveform. For binary black hole signals, sub-dominant modes may contain significant power [47]. A search that includes these modes could, in principle, have an increased reach (and hence event rate) compared to a search that only uses the dominant mode. The EOBNRv2 model of Ref. [15] has been calibrated against higher order modes from numerical relativity simulations. We investigate the effect of ignoring these modes in a search by modeling the BBH signal as an EOBNRv2 signal containing the dominant and sub-dominant multipoles: $h_{lm} = h_{22}, h_{21}, h_{33}, h_{44}, h_{55}$ (which we call EOBNRv2HM) and computing the fitting factor of leading-order EOBNRv2 templates placed using the TaylorF2 metric.

We simulate a population of BBH signals by sampling $100,000$ systems uniformly in the $m_1, m_2 \in [3, 25]\, M_\odot$ component-mass space. These EOBNRv2HM signals are uniformly distributed in sky-location angles and inclination and polarization angles, which appear in the detector's response function to the gravitational-wave signal [69]. The template bank is again placed with a desired minimal match of 0.97 and for each of signal waveforms, we calculate the $\mathcal{FF}$ against the entire bank of EOBNRv2 waveform templates. Fig. 5 shows the value of the $\mathcal{FF}$ of the bank of EOBNRv2 waveform templates at the sampled mass values. As expected, the higest fitting factors are observed close to the equal mass line, since when the mass ratio is close to unity, the amplitude of the sub-leading waveform modes is several orders of magnitude smaller than the amplitude of the dominant mode. As the mass ratio increases, the relative amplitude of the sub-leading multipoles increases, as illustrated by Fig. 1 of Ref. [15] and the

fitting factor decreases. For systems with mass-ratio q above $1.5\,(3.25)$, we find that the $\mathcal{FF}$ of the EOBNRv2 waveform bank is above $0.965\,(0.947)$ over 99.9% of this restricted region. These results demonstrate that the effect of ignoring sub-dominant modes does not cause a significant loss in the total possible signal-to-noise if the mass ratio is less than 1.5. Fitting factors as low as 0.92 are observed in the most asymetric region of the mass space, suggesting that a search that includes higher order modes could achieve a non-trivial increase in sensitivity over leading-order mode templates. However, this needs be evaluated carefully: an algorithm that includes sub-dominant modes could have an increased false-alarm rate (background) over a search that includes only the leading-order mode. Furthermore, it has been found that binaries for which the lowest fitting factors are observed radiate the least energy and hence are those to which the search is least sensitive [47]. Therefore the overall event rate loss from a real BBH signal population may not be as significant as suggested by fitting factor calculations alone.

IV. CONCLUSIONS

We used the TaylorF2 second-order post-Newtonian hexagonal placement algorithm of Refs. [32–34] to construct a template bank of EOBNRv2 waveforms with MM of 0.97. We calculated the fitting factor ($\mathcal{FF}$) of this bank against $\sim 90,000$ simulated EOBNRv2 signals with component masses uniformly distributed between $3M_\odot \leq m_1, m_2 \leq 25M_\odot$. We find that the $\mathcal{FF}$ of the template bank is greater than 0.97 for 98.5% of the simulated EOBNRv2 signals, assuming the zero-detuning high power noise spectrum for aLIGO sensitivity [35]. We conclude that the existing placement algorithm is effectual for use in aLIGO BBH searches, assuming that EOBNRv2 is an accurate model of BBH signals in this mass region. We then demonstrated that use of the computationally cheaper third-and-a-half order TaylorF2 waveform results in a loss in search efficiency due to inaccuracies of the post-Newtonian approximation, and neglect of merger-ringdown for BBHs with a total mass $M > 12\,M_\odot$. However, below this limit the TaylorF2 model is an acceptable signal for BBH serches. This was done using a bank with a MM of 0.97. By increasing the density of the bank to $0.99\mathrm{MM}$, the limit on total-mass can be relaxed to $16\,M_\odot$, with an increase in computational cost due to the number of templates increasing by a factor of ~ 2.7. Finally, we investigated the loss in the SNR incurred by the using template banks constructed using only the leading order mode of EOBNRv2 waveforms. We found that a leading-order EOBNRv2 template bank constructed with a MM of 0.97 is effectual for BBHs searches for which $1 \leq (m_1/m_2) \leq 1.5$ and there is no significant loss in potential signal-to-noise ratio for systems as high as $q = 3.25$. For such systems, using EOBNRv2HM templates is unlikely to give a significant increase in the range to which they can be detected. For BBH with $(m_1/m_2) \geq 3.25$, detection searches could possibly gain sensitivity by the use of EOBNRv2HM waveforms, if they can be implemented without increasing the false alarm rate.

Our results suggest that a significant portion of the non-spinning stellar-mass BBH parameter space can be searched for using LIGO's existing search algorithms. For systems with total mass below $12M_\odot$ template banks of TaylorF2 can be used without significant loss in event rate. For higher mass systems, neglecting high-order modes in an EOBNRv2 search does not cause a substantial reduction in the maximum possible reach of BBH searches. Finally, we note that our study does not consider BBH systems with BH masses higher than $M = 25\,M_\odot$, or the effect of black hole component spins. Future work will extend this study for systems with spinning and/or precessing black holes and consider the effect of non-Gaussian transients in real detector noise.

ACKNOWLEDGMENTS

We are grateful to Stefan Ballmer, Jolien Creighton, Ian Harry, Eliu Huerta, Peter Saulson, and Matt West for helpful comments. We thank Tom Dent for carefully reading this manuscript and Yi Pan for fixing a problem with the EOBNRv2 model discovered during this work. We are grateful to Evan Ochsner and Craig Robinson for writing the LAL implementation of EOBNRv2 against which our code was validated. This work was supported NSF grants PHY-0847611 and PHY-0854812, and a Research Corporation for Science Advancement Cottrell Scholar award. Computations were carried out on the SUGAR cluster which is supported by NSF grants PHY-1040231, PHY-1104371, and PHY-0600953, and by Syracuse University ITS. Part of this work was carried out at the Kavli Institute for Theoretical Physics at Santa Barbara University, supported in part by NSF grant PHY-0551164.

[1] G. M. Harry *et al.* (LIGO Scientific Collaboration), Class.Quant.Grav. **27**, 084006 (2010).

[2] F. Acernese *et al.* (The Virgo Collaboration), "Advanced Virgo Baseline Design," (2009), [Virgo Techincal Document VIR-0027A-09].

[3] K. Somiya (KAGRA Collaboration), Class.Quant.Grav. **29**, 124007 (2012), arXiv:1111.7185 [gr-qc].

[4] S. Waldman (the LIGO Scientific Collaboration), (2011), arXiv:1103.2728 [gr-qc].

[5] S. W. Hawking and W. Israel, *Three Hundred Years of Gravitation* (Cambridge University Press, 1987).

[6] J. Abadie *et al.* (LIGO Scientific Collaboration, Virgo Collaboration), Class.Quant.Grav. **27**, 173001 (2010), arXiv:1003.2480 [astro-ph.HE].

[7] A. Buonanno and T. Damour, Phys.Rev. **D59**, 084006 (1999), arXiv:gr-qc/9811091 [gr-qc].

[8] T. Damour, A. Nagar, M. Hannam, S. Husa, and B. Bruegmann, Phys.Rev. **D78**, 044039 (2008), arXiv:0803.3162 [gr-qc].

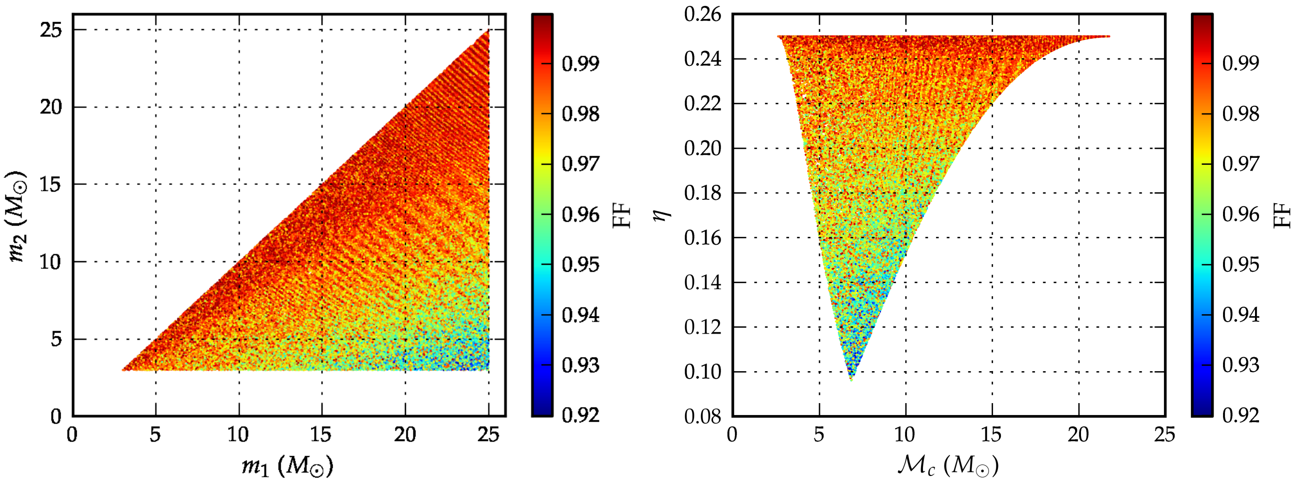

FIG. 5. The $\mathcal{FF}$ of a bank of EOBNRv2 waveforms, constructed with a minimal match of 0.97 at each point in the stellar-mass BBH component-mass region (left), and the same shown on $\mathcal{M}_c - \eta$ axes (right). The color at each point is the value of the $\mathcal{FF}$ of the EOBNRv2 bank at that point against EOBNRv2HM signals.

[9] A. Buonanno, Y. Pan, H. P. Pfeiffer, M. A. Scheel, L. T. Buchman, *et al.*, Phys.Rev. **D79**, 124028 (2009), arXiv:0902.0790 [gr-qc].

[10] T. Damour and A. Nagar, Phys.Rev. **D79**, 081503 (2009), arXiv:0902.0136 [gr-qc].

[11] T. Damour and A. Nagar, Phys.Rev. **D77**, 024043 (2008), arXiv:0711.2628 [gr-qc].

[12] T. Damour, A. Nagar, E. N. Dorband, D. Pollney, and L. Rezzolla, Phys.Rev. **D77**, 084017 (2008), arXiv:0712.3003 [gr-qc].

[13] A. Buonanno and T. Damour, Phys.Rev. **D62**, 064015 (2000), 52 pages, 21 figures, ReVTex, epsfig; few misprints corrected, arXiv:gr-qc/0001013 [gr-qc].

[14] T. Damour, B. R. Iyer, P. Jaranowski, and B. Sathyaprakash, Phys.Rev. **D67**, 064028 (2003), arXiv:gr-qc/0211041 [gr-qc].

[15] Y. Pan, A. Buonanno, M. Boyle, L. T. Buchman, L. E. Kidder, *et al.*, Phys.Rev. **D84**, 124052 (2011), 26 pages, 25 figures, arXiv:1106.1021 [gr-qc].

[16] E. Berti, V. Cardoso, and C. M. Will, Phys.Rev. **D73**, 064030 (2006), arXiv:gr-qc/0512160 [gr-qc].

[17] Y. Mino, M. Sasaki, M. Shibata, H. Tagoshi, and T. Tanaka, Prog.Theor.Phys.Suppl. **128**, 1 (1997), arXiv:gr-qc/9712057 [gr-qc].

[18] J. Abadie *et al.* (LIGO Scientific Collaboration, Virgo Collaboration), Phys.Rev. **D85**, 082002 (2012), arXiv:1111.7314 [gr-qc].

[19] J. Abadie *et al.* (LIGO Scientific Collaboration, Virgo Collaboration), Phys.Rev. **D82**, 102001 (2010), arXiv:1005.4655 [gr-qc].

[20] B. Abbott *et al.* (LIGO Scientific Collaboration), Phys.Rev. **D80**, 047101 (2009), arXiv:0905.3710 [gr-qc].

[21] B. Abbott *et al.* (LIGO Scientific Collaboration), Phys.Rev. **D79**, 122001 (2009), arXiv:0901.0302 [gr-qc].

[22] E. Messaritaki (LIGO Scientific Collaboration), Class.Quant.Grav. **22**, S1119 (2005), arXiv:gr-qc/0504065 [gr-qc].

[23] L. A. Wainstein and V. D. Zubakov, *Extraction of signals from noise* (Prentice-Hall, Englewood Cliffs, NJ, 1962).

[24] B. Allen *et al.*, (2005), arXiv:gr-qc/0509116 [gr-qc].

[25] F. Ozel, D. Psaltis, R. Narayan, and J. E. McClintock, Astrophys.J. **725**, 1918 (2010), arXiv:1006.2834 [astro-ph.GA].

[26] B. Sathyaprakash and S. Dhurandhar, Phys.Rev. **D44**, 3819 (1991).

[27] R. Balasubramanian, B. Sathyaprakash, and S. Dhurandhar, Phys.Rev. **D53**, 3033 (1996), arXiv:gr-qc/9508011 [gr-qc].

[28] T. Apostolatos, Phys.Rev. **D52**, 605 (1995).

[29] K. Cannon *et al.*, Phys.Rev. **D82**, 044025 (2010).

[30] B. J. Owen, Phys.Rev. **D53**, 6749 (1996), arXiv:gr-qc/9511032 [gr-qc].

[31] B. Sathyaprakash, Phys.Rev. **D50**, 7111 (1994), arXiv:gr-qc/9411043 [gr-qc].

[32] S. Babak, R. Balasubramanian, D. Churches, T. Cokelaer, and B. Sathyaprakash, Class.Quant.Grav. **23**, 5477 (2006), arXiv:gr-qc/0604037 [gr-qc].

[33] B. J. Owen and B. Sathyaprakash, Phys.Rev. **D60**, 022002 (1999), arXiv:gr-qc/9808076 [gr-qc].

[34] T. Cokelaer, Phys.Rev. **D76**, 102004 (2007), arXiv:0706.4437 [gr-qc].

[35] LIGO (David Shoemaker), *Advanced LIGO anticipated sensitivity curves*, Tech. Rep. (LIGO Document T0900288-v3, 2009).

[36] C. Cutler and E. E. Flanagan, Phys.Rev. **D49**, 2658 (1994), arXiv:gr-qc/9402014 [gr-qc].

[37] S. Droz, D. J. Knapp, E. Poisson, and B. J. Owen, Phys.Rev. **D59**, 124016 (1999), arXiv:gr-qc/9901076 [gr-qc].

[38] L. Blanchet, T. Damour, G. Esposito-Farese, and B. R. Iyer, Phys.Rev.Lett. **93**, 091101 (2004), arXiv:gr-qc/0406012 [gr-qc].

[39] L. Blanchet and B. R. Iyer, Phys.Rev. **D71**, 024004 (2005), arXiv:gr-qc/0409094 [gr-qc].

[40] P. Jaranowski and G. Schaefer, Annalen Phys. **9**, 378 (2000), arXiv:gr-qc/0003054 [gr-qc].

[41] P. Jaranowski and G. Schaefer, Phys.Rev. **D60**, 124003 (1999), arXiv:gr-qc/9906092 [gr-qc].

[42] T. Damour, P. Jaranowski, and G. Schaefer, Phys.Lett. **B513**, 147 (2001), arXiv:gr-qc/0105038 [gr-qc].

[43] L. E. Kidder, Phys.Rev. **D77**, 044016 (2008), arXiv:0710.0614 [gr-qc].

[44] L. Blanchet, G. Faye, B. R. Iyer, and S. Sinha, Class.Quant.Grav. **25**, 165003 (2008), 57 pages, no figures, arXiv:0802.1249 [gr-qc].

[45] A. Buonanno, B. Iyer, E. Ochsner, Y. Pan, and B. Sathyaprakash, Phys.Rev. **D80**, 084043 (2009), arXiv:0907.0700 [gr-qc].

[46] D. McKechan, (2011), ph.D. thesis, arXiv:1102.1749 [gr-qc].

[47] L. Pekowsky, J. Healy, D. Shoemaker, and P. Laguna, (2012), arXiv:1210.1891 [gr-qc].

[48] L. Blanchet, Living Rev.Rel. **9**, 4 (2006).

[49] F. Pretorius, Phys.Rev.Lett. **95**, 121101 (2005), arXiv:gr-qc/0507014 [gr-qc].

[50] F. Pretorius, Class.Quant.Grav. **23**, S529 (2006), arXiv:gr-qc/0602115 [gr-qc].

[51] M. A. Scheel, M. Boyle, T. Chu, L. E. Kidder, K. D. Matthews, *et al.*, Phys.Rev. **D79**, 024003 (2009), arXiv:0810.1767 [gr-qc].

[52] J. A. Gonzalez, U. Sperhake, and B. Bruegmann, Phys.Rev. **D79**, 124006 (2009), arXiv:0811.3952 [gr-qc].

[53] D. Pollney, C. Reisswig, E. Schnetter, N. Dorband, and P. Diener, Phys.Rev. **D83**, 044045 (2011), arXiv:0910.3803 [gr-qc].

[54] C. O. Lousto, H. Nakano, Y. Zlochower, and M. Campanelli, Phys.Rev.Lett. **104**, 211101 (2010), arXiv:1001.2316 [gr-qc].

[55] L. T. Buchman, H. P. Pfeiffer, M. A. Scheel, and B. Szilagyi, (2012), arXiv:1206.3015 [gr-qc].

[56] P. Ajith, M. Boyle, D. A. Brown, B. Brugmann, L. T. Buchman, *et al.*, Class.Quant.Grav. **29**, 124001 (2012), arXiv:1201.5319 [gr-qc].

[57] T. Damour, P. Jaranowski, and G. Schaefer, Phys.Rev. **D62**, 084011 (2000), arXiv:gr-qc/0005034 [gr-qc].

[58] T. Damour, B. R. Iyer, and A. Nagar, Phys.Rev. **D79**, 064004 (2009), arXiv:0811.2069 [gr-qc].

[59] A. Buonanno and T. Damour, Phys.Rev. **D59**, 084006 (1999), arXiv:gr-qc/9811091 [gr-qc].

[60] "LSC Algorithm Library," `https://www.lsc-group.phys.uwm.edu/daswg/projects/lalsuite.html`.

[61] J. Mathews and R. L. Walker, *Mathematical Methods of Physics* (W.A. Benjamin; 2nd edition, 1970).

[62] L. Blanchet, T. Damour, B. R. Iyer, C. M. Will, and A. Wiseman, Phys.Rev.Lett. **74**, 3515 (1995), arXiv:gr-qc/9501027 [gr-qc].

[63] L. Blanchet, G. Faye, B. R. Iyer, and B. Joguet, Phys.Rev. **D65**, 061501 (2002), arXiv:gr-qc/0105099 [gr-qc].

[64] L. Blanchet, T. Damour, G. Esposito-Farese, and B. R. Iyer, Phys.Rev.Lett. **93**, 091101 (2004), arXiv:gr-qc/0406012 [gr-qc].

[65] E. Poisson and C. M. Will, Phys.Rev. **D52**, 848 (1995), arXiv:gr-qc/9502040 [gr-qc].

[66] L. Lindblom, B. J. Owen, and D. A. Brown, Phys.Rev. **D78**, 124020 (2008), arXiv:0809.3844 [gr-qc].

[67] L. Lindblom, J. G. Baker, and B. J. Owen, Phys.Rev. **D82**, 084020 (2010), arXiv:1008.1803 [gr-qc].

[68] A. Buonanno, Y. Pan, J. G. Baker, J. Centrella, B. J. Kelly, *et al.*, Phys.Rev. **D76**, 104049 (2007), arXiv:0706.3732 [gr-qc].

[69] B. Sathyaprakash and B. Schutz, Living Rev.Rel. **12**, 2 (2009), arXiv:0903.0338 [gr-qc].